

## Tidal modulation of seabed light and its implications for benthic algae

Roberts, Emyr; Bowers, David; Davies, Andrew

### Limnology and Oceanography

DOI:  
[10.1002/lno.10616](https://doi.org/10.1002/lno.10616)

Published: 01/01/2018

Publisher's PDF, also known as Version of record

[Cyswllt i'r cyhoeddiad / Link to publication](#)

*Dyfyniad o'r fersiwn a gyhoeddwyd / Citation for published version (APA):*  
Roberts, E., Bowers, D., & Davies, A. (2018). Tidal modulation of seabed light and its implications for benthic algae. *Limnology and Oceanography*, 63(1), 91-106.  
<https://doi.org/10.1002/lno.10616>

#### Hawliau Cyffredinol / General rights

Copyright and moral rights for the publications made accessible in the public portal are retained by the authors and/or other copyright owners and it is a condition of accessing publications that users recognise and abide by the legal requirements associated with these rights.

- Users may download and print one copy of any publication from the public portal for the purpose of private study or research.
- You may not further distribute the material or use it for any profit-making activity or commercial gain
- You may freely distribute the URL identifying the publication in the public portal ?

#### Take down policy

If you believe that this document breaches copyright please contact us providing details, and we will remove access to the work immediately and investigate your claim.

## Tidal modulation of seabed light and its implications for benthic algae

Emyr Martyn Roberts ,\* David George Bowers, Andrew John Davies 

School of Ocean Sciences, Bangor University, Menai Bridge, Anglesey, UK

### Abstract

The temporal behavior of seabed light in a shallow, tidal sea is set largely by the interaction of the solar elevation cycle with tidal cycles in water depth and temporal variability in water clarity. The effect of tidal modulation on seabed light often does not simply average out, producing instead a net effect (either an amplification or a reduction of seabed light, integrated over time) compared to a tideless, but otherwise equivalent, scenario. Observations of this phenomenon from the Bay of Brest (France) show reasonable agreement with predictions based on an earlier theoretical framework, confirming that the key physics has been understood and that the important parameters are tidal amplitude, timing of low waters, diffuse attenuation coefficient, and daylength. Implications for benthic macroalgae living in the bay's shallow subtidal zone are investigated using a simple numerical model. The effects of the tide on time-integrated seabed light and, in turn, time-integrated macroalgal community photosynthesis in the Bay of Brest correspond closely at three timescales: annual, springs-neaps (i.e., approximately fortnightly), and daily. Tidal amplification of both parameters occurs over the year, during winter months generally, and at spring tides during winter specifically (slight reduction occurs at neaps during winter). For an individual, isolated thallus, the relationship between tidal modulation of seabed light and photosynthesis is complicated by more pronounced light-saturation and photoinhibition effects. Demonstrated here for the first time, neglecting tidal effects on seabed light is likely to result in erroneous estimates (and, for many sites, underestimation) of subtidal benthic productivity.

Shallow-water benthic ecosystems, such as kelp forests and seagrass meadows, can be highly productive (Mann 1972). They also serve as nurseries, habitats, and refugia for many species of marine fauna (Steneck et al. 2002; Heck et al. 2003). Light availability is often the most important abiotic factor regulating the growth patterns, distribution, and primary productivity of benthic algae and plants (Zimmerman et al. 1994, and references therein). As noted by Ackleson (2003), we must continue to refine our understanding of the influence of seabed light on these ecosystems if we are to better predict their response to short-term changes (e.g., storms and pollution events) and long-term changes (e.g., climate and sea-level), and if we are to better quantify their role within the global ocean carbon cycle.

In a tideless (or “non-tidal”) sea, irradiance at the seabed is controlled largely by the daily and seasonal cycles of solar elevation, which govern sea surface irradiation, and by the water depth and clarity, which together determine the

extent to which incident light is attenuated before it reaches the bed (Bowers and Brubaker 2010). In a “tidal” sea, cycles in water depth (and any associated cycles in water clarity) produce more complicated temporal patterns in seabed irradiance (e.g., Topliss et al. 1980; Pilgrim and Millward 1989; Bowers et al. 1997; Bowers and Brubaker 2004). While these patterns may influence the behavior of benthic animals (Naylor 2010) and the time course of benthic photosynthesis (Gévaert et al. 2002, 2003), the principal value of such tidal modulation lies in its potential to result in a net effect on seabed irradiance (and photosynthesis) integrated over time (Bowers and Brubaker 2010).

Bowers and Brubaker (2010) hypothesized that the tide will tend to amplify the daily total seabed irradiance compared to a scenario with no tide, but with the same mean depth and clarity. They reasoned that light is attenuated in an approximately exponential manner with increasing water depth, and so the “gains” in irradiance around low-waters should exceed the “losses” around high-waters (see Fig. 1), leading to a net gain, or amplification, over time (relative to the “non-tidal” scenario). They went on to demonstrate that the effect is more complicated than the initial premise. The tide can also reduce the daily total seabed irradiance, and the magnitude of the effect depends upon four key parameters: the time of low water, the tidal

\*Correspondence: emyr.roberts@bangor.ac.uk

This is an open access article under the terms of the Creative Commons Attribution License, which permits use, distribution and reproduction in any medium, provided the original work is properly cited.

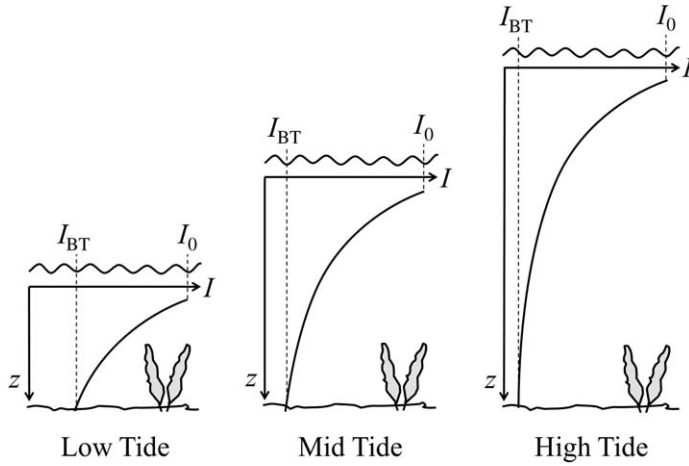


**Fig. 1.** Schematic demonstrating how the exponential attenuation of irradiance,  $I$ , with depth,  $z$ , can lead to tidal amplification (after Bowers and Brubaker 2010). The disproportionately large “gain” in tidally modulated seabed irradiance,  $I_{BT}$ , at low tide (compared to that at mid tide) is not matched by the similarly defined “loss” at high tide. The magnitude of the amplification will depend upon the diffuse attenuation coefficient,  $k_{PAR}$  (which controls the rate of exponential attenuation with depth), and the tidal range,  $R$ . Sea surface irradiance,  $I_0$ , varies throughout the day (not illustrated), meaning that the timing of low waters,  $t_{lw}$ , and the daylength,  $L$ , are also important.

amplitude (or range), the diffuse attenuation coefficient (a measure of the turbidity of the water), and the daylength.

The ecological implications of the study by Bowers and Brubaker (2010) were potentially very significant, and warrant further investigation. In particular, models that ignore the tide (and use instead a mean water depth) were claimed to underestimate seabed irradiance and may, therefore, also underestimate benthic primary production. Given that the relationship between irradiance and photosynthesis is non-linear (see “Theory” below and standard texts such as Hurd et al. 2014), it is unclear whether a large tidal amplification of seabed light will cause a similar amplification of photosynthesis in benthic algae: gains in irradiance at low water will not necessarily result in equivalent gains in photosynthesis if saturation or photoinhibition occur.

The purpose of the present paper is twofold: (1) to test the original theory against irradiance observations from a new site, the Bay of Brest in France (n.b., the theory has thus far been validated using data from one site only, the Menai Strait in Wales, UK), and (2) to further investigate the ecological implications of Bowers and Brubaker (2010) by the construction of a simple numerical model.

The Bay of Brest was selected on the basis that it is a macrotidal site with tidal and turbidity characteristics that differ from those of the Menai Strait. The Bay of Brest is less turbid, and low waters of spring tides (LWST) always occur at about midday and midnight (i.e., opposite to the case at the Menai Strait, where high waters of spring tides (HWST) occur at these times). Large tidal ranges at spring tides and the

coincidence of LWST with the midday peak in sea surface irradiance create a potential for large tidal irradiance amplification. A novel mooring design was employed to measure, rather than infer (as in the original study), “non-tidal” irradiance. The numerical model has been used to investigate the likely effect of the tide on seabed irradiance and benthic photosynthesis in the Bay of Brest over three timescales (i.e., daily, springs-neaps cycle, and annual) and for two ecological entities (i.e., the individual, isolated kelp thallus, and the established macroalgal community).

## Theory

### Tidal irradiance amplification

Irradiance at the seabed,  $I_B$ , is given by the Lambert-Beer Law,

$$I_B(t) = I_0(t) \exp[-k_{PAR}(t)z(t)], \quad (1)$$

where  $I_0$  is the sea surface irradiance,  $k_{PAR}$  is the diffuse attenuation coefficient of photosynthetically active radiation (PAR),  $z$  is the water depth, and  $t$  is time. The law typically applies to monochromatic light, but it also applies approximately to irradiance integrated over the PAR waveband (i.e., approximately 400–700 nm) (Kirk 1994), as required here. Daily total seabed irradiance is determined by integrating the expression above over time.

Bowers and Brubaker (2010) defined a daily tidal irradiance amplification factor,  $F$ , as the ratio of the daily total seabed irradiance in a “tidal” scenario to that in an equivalent “non-tidal” scenario. Initially, they represented tidal variation in water depth as  $z_T = z_0 - b \cos(\omega(t - t_{lw}))$ , where  $z_0$  is the mean water depth,  $b$  is the tidal amplitude,  $\omega$  is the angular frequency of the tide (approximately  $0.5 \text{ rad h}^{-1}$  for a semi-diurnal tide),  $t$  is time and  $t_{lw}$  is the time of low water (both measured relative to midday). Water depth in the equivalent non-tidal scenario,  $z_{NT}$ , was taken to be  $z_0$ .  $F$  was therefore given as

$$F = \frac{\langle I_{BT} \rangle}{\langle I_{BNT} \rangle} \quad (2)$$

$$= \frac{\int_{-L/2}^{L/2} I_0(t) \exp[-k_{PAR}(t)(z_0 - b \cos(\omega(t - t_{lw})))] dt}{\int_{-L/2}^{L/2} I_0(t) \exp[-k_{PAR}(t)z_0] dt}, \quad (3)$$

where the subscripts  $T$  and  $NT$  represent “tidal” and “non-tidal” parameters respectively, and angular brackets denote daily totals. Since times are measured relative to midday and  $L$  is the daylength, the limits of integration are from  $-L/2$  (dawn) to  $L/2$  (dusk).  $F > 1$  indicates tidal amplification of seabed light,  $F < 1$  indicates tidal reduction, and  $F = 1$  indicates that the tide makes no discernible difference.

Equation 3 can be solved numerically regardless of how  $I_0$  and  $k_{PAR}$  are varied over the day. However, Bowers and

Brubaker (2010) found that an approximate analytical solution can be obtained by making a number of simplifying assumptions. First,  $k_{\text{PAR}}$  is treated as a constant over the day; to this end, a daily mean value,  $\bar{k}_{\text{PAR}}$ , suffices. Second, sea surface irradiance is approximated using a Gaussian curve,  $I_0(t) = I_M \exp[-(t/q)^2]$ , where  $I_M$  is the maximum (i.e., mid-day) surface irradiance,  $t$  is time (again measured relative to midday), and  $q$  is a parameter that controls the width of the Gaussian curve ( $q \approx L/3$  offers a reasonable fit to observations of  $I_0$  (Bowers and Brubaker 2004)). Finally, tidally varying water depth,  $z_T$ , is (re-)approximated as a parabola about low water by expanding the cosine term into its equivalent power series and retaining the first two terms only. That is,  $z_T = z_0 - b(1 - \omega^2(t - t_{\text{lw}})^2/2)$ .

Substituting the above approximations into Eq. 3 ensures that both the integral in the numerator and that in the denominator have solvable forms, leading to the following analytical solution:

$$F = \sqrt{\frac{1}{x+1}} \exp[\bar{k}_{\text{PAR}}b] (\exp[-\phi_1] + \exp[-\phi_2]), \quad (4)$$

where  $x = 0.5\bar{k}_{\text{PAR}}b\omega^2q^2$ , and  $\phi = (x/(x+1))(t_{\text{lw}}/q)^2$ . Subscripts 1 and 2 on  $\phi$  refer to its calculation using the time of either the first or second low water occurring in a day, respectively.

We have not reproduced here all intermediate steps in the derivation of this analytical solution. For these, the interested reader is referred to Bowers and Brubaker (2010).

### Tidal photosynthesis amplification

A daily tidal photosynthesis amplification factor,  $\Psi$ , may be defined such that it is analogous to the daily tidal irradiance amplification factor,  $F$ .

$$\Psi = \frac{\langle P_{\text{BT}} \rangle}{\langle P_{\text{BNT}} \rangle} \quad (5)$$

$$= \frac{\int_{-L/2}^{L/2} P_{\text{BT}}(t) dt}{\int_{-L/2}^{L/2} P_{\text{BNT}}(t) dt}, \quad (6)$$

where  $P$  is the rate of (benthic algal) photosynthesis, subscripts denote either a “tidal” or a “non-tidal” parameter, angular brackets denote daily totals of the enclosed parameters, and  $L$  is daylength.  $\Psi > 1$  indicates tidal amplification of daily total seabed photosynthesis,  $\Psi < 1$  indicates a tidal reduction, and  $\Psi = 1$  indicates that the tide produces no discernible difference.

### Photosynthesis-irradiance ( $P$ - $I$ ) curve equations

Data analysis and modeling aspects of this work are repeated using two different  $P$ - $I$  curve parameterizations (Fig. 2): (1) the Peeters and Eilers (1978) Model, and (2) the Lederman and Tett (1981) Model.

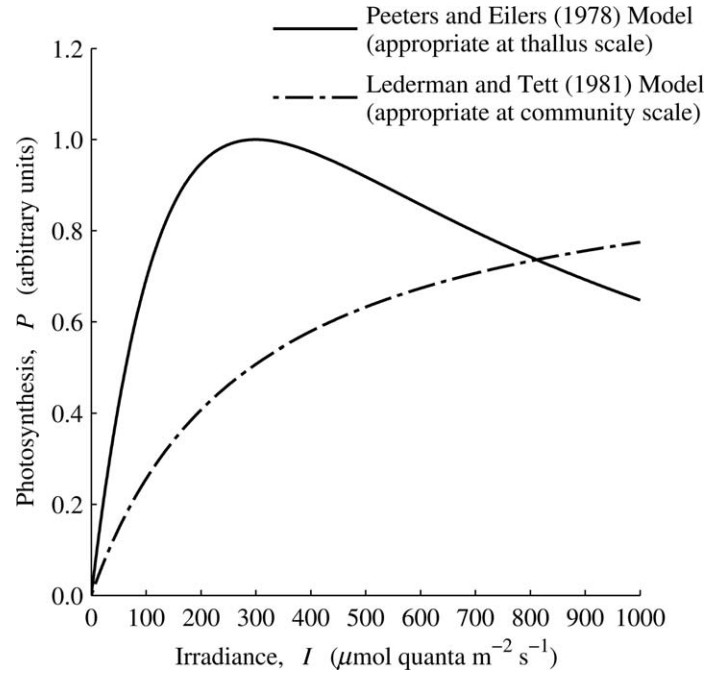


**Fig. 2.** Photosynthesis-irradiance ( $P$ - $I$ ) curves generated using the two equations employed in this study. The Peeters and Eilers (1978) Model (Eq. 7) is appropriate for thallus-scale photosynthesis, and input values used to produce the curve are representative of *Saccharina latissima* (values from Gévaert et al. 2003). The Lederman and Tett (1981) Model (Eq. 8) is appropriate for macroalgal community-scale photosynthesis, and input values used were from Middelboe et al. (2006). See Table 1 for input values.

The Peeters and Eilers (1978)  $P$ - $I$  Model is appropriate at the thallus scale. It is mechanistic (rather than empirically derived) and includes the effect of photoinhibition. It has been used successfully to fit observed  $P$ - $I$  curves for a common subtidal kelp species (*Saccharina latissima*) near our study site in Brittany (Gévaert et al. 2003). *Saccharina latissima* is found in the Bay of Brest (Hily et al. 1992) and is an excellent subject for the purpose of inferring/modeling photosynthesis in the subtidal zone.

Middelboe et al. (2006) found that, unlike for isolated thalli, the photosynthetic production of established macroalgal communities in shallow water tends not to become fully light-saturated or photoinhibited at the highest incident irradiances. The authors attributed this to a number of reasons associated with the species richness/composition of the community, and with canopy structure and density. We therefore repeat our analyses using the Lederman and Tett (1981) “Rectangular Hyperbola”  $P$ - $I$  Model (i.e., no true saturation, no photoinhibition), which Middelboe et al. (2006) used successfully to fit the  $P$ - $I$  responses of shallow-water macroalgal communities off Denmark.

Both equations are given below, and we use the subscripts  $t$  and  $c$  to denote “thallus-scale” and “community-scale” parameters, respectively. Note that throughout the present work we have effectively normalized rates of thallus and community photosynthesis by their respective maxima.

**Table 1.** Input parameters and their values for the numerical model. Surface irradiance and tidal parameters were selected to be representative of the Bay of Brest. Photosynthesis parameters were selected to be representative of a thallus of *Saccharina latissima* or an established macroalgal community (see text).

Parameter	Symbol(s)	Value
<i>Sea surface irradiance parameters</i>		
Latitude of Bay of Brest	$\gamma$	48.3°
Solar constant (PAR component)*	$I_{SC}$	2400 $\mu\text{mol}$ quanta $\text{m}^{-2} \text{s}^{-1}$
Atmospheric attenuation coeff.	$k_{\text{Atmos}}$	0.01
<i>Tidal cycle parameters</i>		
$M_2$ period	-	12.421 h
$S_2$ period	-	12 h
$M_2$ amplitude	-	2.1 m
$S_2$ amplitude	-	1.0 m
$M_2$ phase	-	0°
$S_2$ phase	-	180°
<i><math>\bar{k}_{\text{PAR}}</math> variation parameters (dependence on <math>\bar{R}</math>)</i>		
Max. (winter) gradient	$m$	0.1 $\text{m}^{-2}$
Intercept	$c$	0.4 $\text{m}^{-1}$
<i>Photosynthesis parameters</i>		
Max. rate of photosyn.	$P_{m,t}, P_{m,c}$	1 (arbitrary units)
Optimum irradiance <sup>†</sup>	$I_{m,t}$	300 $\mu\text{mol}$ quanta $\text{m}^{-2} \text{s}^{-1}$
Saturation onset irradiat. <sup>†</sup>	$I_{k,t}$	100 $\mu\text{mol}$ quanta $\text{m}^{-2} \text{s}^{-1}$
Saturation onset irradiat. <sup>‡</sup>	$I_{k,c}$	291 $\mu\text{mol}$ quanta $\text{m}^{-2} \text{s}^{-1}$

\* A solar constant of 1373  $\text{W m}^{-2}$  (total solar irradiance) is assumed, of which approximately 38% (521.74  $\text{W m}^{-2}$ ) is PAR (Kirk 1994). This is multiplied by the approximate conversion factor 4.6  $\mu\text{mol quanta J}^{-1}$ , which arises from assuming PAR has a mean wavelength of 550 nm, to provide the PAR component in the appropriate units for this study.

<sup>†</sup> Approximated from Gévaert et al. (2003), and applied to the thallus-scale  $P-I$  equation (Eq. 7).

<sup>‡</sup> Value from Middelboe et al. (2006), and applied to the community-scale  $P-I$  equation (Eq. 8).

Thus, the maximum (“normalized”) photosynthesis achievable has a value of 1 in both cases. This has the benefit that both thallus and community photosynthesis can be plotted on the same axis or using the same scale for straightforward comparison. We have expressed this “normalized” photosynthesis in arbitrary units, which are dimensionless. Values input into the equations are given in Table 1. The Peeters and Eilers (1978) equation is as follows:

$$P_t = \frac{I}{aI^2 + bI + c}, \quad (7)$$

where the coefficients  $a$ ,  $b$ , and  $c$  dictate the precise shape of the curve. These are, in turn, functions of key photosynthesis parameters, as follows:

$$a = \frac{1}{\alpha_t I_{m,t}^2},$$

$$b = \frac{1}{P_{m,t}} - \frac{2}{\alpha_t I_{m,t}},$$

and

$$c = \frac{1}{\alpha_t},$$

where  $\alpha_t = P_{m,t}/I_{k,t}$  (i.e., the initial slope of the  $P-I$  curve, or light use efficiency),  $P_{m,t}$  is the maximum possible rate of photosynthesis (n.b., in this study,  $P_t$  is the “normalized” thallus photosynthesis discussed above, expressed in dimensionless arbitrary units, and thus we assign to  $P_{m,t}$  a value of 1),  $I_{k,t}$  is the saturation onset irradiance (i.e., the irradiance threshold beyond which photosynthesis begins to become light-saturated, or, more formally, the irradiance at which the initial slope of the  $P-I$  curve (extrapolated) intersects the maximum rate of photosynthesis,  $P_{m,t}$ ), and  $I_{m,t}$  is the optimum irradiance (i.e., the irradiance at which  $P_{m,t}$  is achieved).

The Lederman and Tett (1981) equation is as follows:

$$P_c = \frac{\alpha_c P_{m,c} I}{P_{m,c} + \alpha_c I}, \quad (8)$$

where  $\alpha_c = P_{m,c}/I_{k,c}$  (i.e., the initial slope of the  $P-I$  curve, or community light use efficiency),  $P_{m,c}$  is the maximum photosynthesis achievable (n.b.,  $P_c$  is the “normalized” community photosynthesis discussed above, expressed in dimensionless arbitrary units, and thus we assign to  $P_{m,c}$  a value of 1), and  $I_{k,c}$  is the saturation onset irradiance for the community.

## Materials and methods

### Study site

The Bay of Brest (Fig. 3) is located at the westernmost extremity of the Brittany Peninsula in Northwest France, and has an area of approximately 180  $\text{km}^2$ . It is connected to the Iroise Sea and the Atlantic Ocean beyond via a narrow, shallow channel (about 1.8 km wide, 4 km long, and, at its deepest, 50 m deep), known locally as “Le Goulet.” The bay itself is shallower, with wide shoals and a mean depth of 10 m (Monbet and Bassoullet 1989; Thouzeau et al. 2000).

The hydrodynamics of the Bay of Brest are dominated by tidal forcing. The average tidal range is 4.2 m, and ranges of up to 7.5 m are reached at large spring tides (Monbet and Bassoullet 1989). Consequently, large exchanges of water occur through Le Goulet, and tidal currents there reach speeds of up to 2  $\text{m s}^{-1}$  (Salomon and Breton 1991). Freshwater input to the Bay of Brest (through the Éloron and Aulne Rivers) is small compared to the tidal exchanges with the

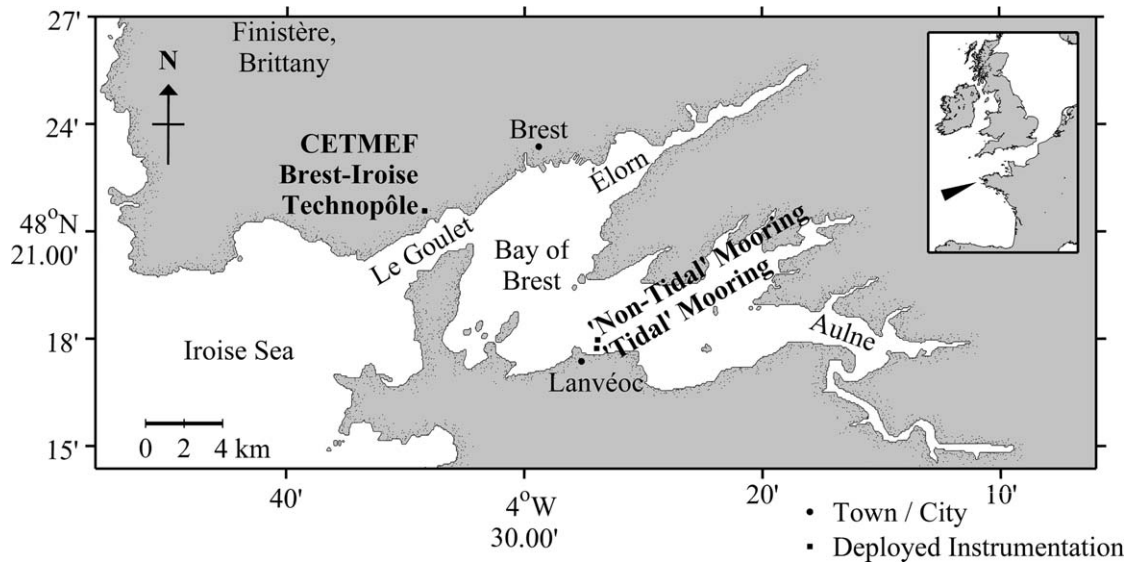


**Fig. 3.** The Bay of Brest study site at the western extremity of the Brittany Peninsula (inset). Deployed instrumentation is indicated with black squares and a bold typeface (see text for details).

Iroise Sea (Monbet and Bassoulet 1989), and the bay is typically well-mixed (Delmas and Tréguer 1983).

The phase of the solar semi-diurnal (or  $S_2$ ) tidal constituent at the Bay of Brest is approximately  $180^\circ$  (expressed as a phase lag behind the corresponding constituent of the equilibrium tide at Greenwich) (Pingree and Griffiths 1981). Consequently, the low waters of spring tides (LWST) always occur at about midday and midnight; at neaps, high waters occur at these times. Daylength at the site varies from approximately 8 h in winter to 16 h in summer (calculated for the latitude of the study site using equations from Kirk 1994). The Bay of Brest is less turbid than the Menai Strait (G. Chapalain pers. comm.; Roberts et al. 2014). It can, however, still be considered “coastal” in optical water type.

**Observational campaigns**

Fieldwork campaigns were undertaken in summer (July 2011) and winter (December 2011), and were approximately 2 and 3 weeks in length, respectively. During each campaign, two moorings were deployed simultaneously (as illustrated in Fig. 4) in the southern part of the Bay of Brest, near the town of Lanvéoc (see Fig. 3).

Tidally modulated seabed irradiance,  $I_{BT}$ , was measured using an irradiance sensor in a bed frame (Fig. 4). This we will refer to as the “tidal” mooring or condition. The sensor was fixed at 1.5 m above the seabed, and the frame was deployed in sufficiently deep water that it remained submerged at all stages of the tide. Its position was  $48^\circ 17.55'N$   $4^\circ 26.96'W$  (see Fig. 3). A pressure sensor was fixed to the frame to allow the (tidally varying) water depth,  $z_T$ , above the irradiance sensor to be monitored.

Irradiance beneath a fixed depth of water,  $I_{BNT}$ , was measured by suspending an identical irradiance sensor beneath a

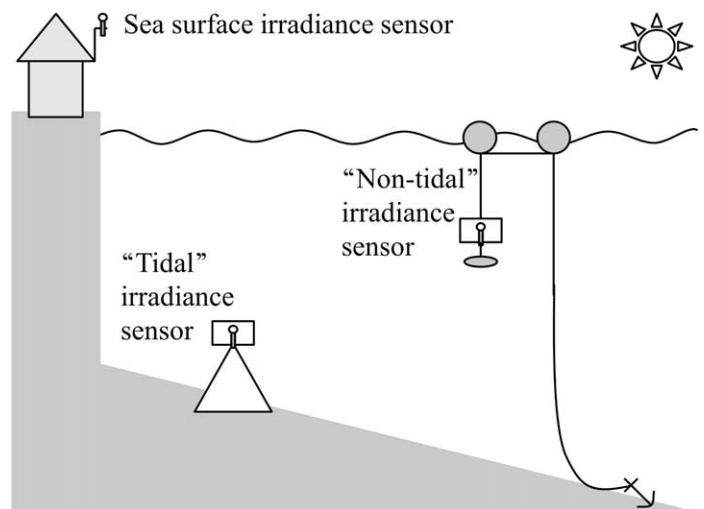


**Fig. 4.** Schematic of the moorings deployed to observe tidal irradiance amplification.

surface buoy (Fig. 4). The buoy and instrument were free to move vertically up and down with the sea surface, but the sensor remained submerged beneath a relatively constant depth of water,  $z_{NT}$ . We will refer to this as the “non-tidal” mooring or condition. Its position was  $48^\circ 17.79'N$   $4^\circ 26.92'W$  (see Fig. 3). A pressure sensor was fitted to this mooring also, to check that variability in  $z_{NT}$  remained acceptably low. Several novel features were incorporated into the design of the “non-tidal” mooring. These features helped to reduce instrument line swing/lean, to prevent excessive slack in the tether, and to permit the mooring to align freely with changing current directions. They are described fully in

Roberts (2015). The combined effect was to maintain a relatively constant instrument depth and to prevent mooring self-entanglement.

Sea surface irradiance,  $I_0$ , was monitored using a third sensor positioned on the roof of the Centre d'Études Techniques Maritimes et Fluviales (CETMEF) at the Brest-Iroise Technopôle (48° 21.52'N 4° 34.01'W, Fig. 3). Prior to each fieldwork campaign, all sensors (i.e., irradiance and pressure sensors) were set to log measurements synchronously every 2 min.

We required that the contrived “non-tidal” condition be comparable with the “tidal” condition in terms of both mean water depth and clarity. The instrument on the “non-tidal” mooring was positioned at a depth equal to the mean depth experienced by the “tidal” instrument. This was determined in advance of deployment using tide tables, and verified after recovery using the pressure (depth) records. Both moorings were positioned as close together as was practically possible, so that they might experience similar conditions of water clarity. The “non-tidal” mooring, however, was necessarily deployed in deeper water (i.e., further offshore) so that its instrument was not grounded at low water.

A Lambert-Beer Law-based correction was applied to the  $I_{\text{BNT}}$  data to account for the fact that daily mean attenuation coefficients,  $\bar{k}_{\text{PAR}}$ , at the site of the “non-tidal” mooring were consistently lower than at the site of the “tidal” bed frame (in shallower, more turbid water). Time series of instantaneous  $k_{\text{PAR}}$  were calculated for both the “tidal” and “non-tidal” scenarios by using observations of sea surface irradiance, seabed irradiance, and water depth to solve Eq. 1 for  $k_{\text{PAR}}$ . Daily means,  $\bar{k}_{\text{PAR}}$ , were determined for both scenarios and the differences between corresponding daily means,  $\Delta\bar{k}_{\text{PAR}}$  ( $=\bar{k}_{\text{PAR,tidal}}-\bar{k}_{\text{PAR,non-tidal}}$ ), were used to correct (reduce) the appropriate instantaneous  $I_{\text{BNT}}$  values, according to  $I_{\text{BNT,corrected}}(t) = I_{\text{BNT,original}}(t)\exp[-\Delta\bar{k}_{\text{PAR}}z_{\text{NT}}(t)]$ . This correction effectively equates the daily mean attenuation coefficients of the two scenarios, while preserving the natural variability of the records.

The irradiance sensors were of type MDS-MkV/L (JFE Advantech, Kobe, Japan), which measure, and log internally, quantum scalar irradiance in the PAR waveband. Quantum scalar irradiance is the integral of the radiance distribution at a point, over all directions about that point (Kirk 1994). Each instrument had been calibrated by the manufacturer against an LI-189 (LI-COR Biotechnology, Lincoln, Nebraska, U.S.A.) reference sensor, using a halogen light source. The manufacturers claim an accuracy of  $\pm 4\%$  (full scale). Instrument resolution is  $1 \mu\text{mol quanta m}^{-2} \text{s}^{-1}$ . The irradiance sensors used for this study were intercalibrated over a typical daily irradiance range at the School of Ocean Sciences (Bangor University, Wales).

Additional corrections were applied to the irradiance data: (1) the typical dark current reading was deducted from all measurements before further analysis (after Topliss et al. 1980); (2) measurements from the two submerged sensors were multiplied by an “immersion coefficient” to account for the

so-called “immersion effect” (Kirk 1994); and (3) linear intercalibration equations (with coefficients that were averages of those determined pre- and post-fieldwork) were applied to account for slight differences in instrument sensitivities. Furthermore, a green-brown biofilm began to develop on the submerged irradiance collectors after 2 weeks of summertime (July) deployment. The affected records were curtailed (post-recovery) at a length of 13 d to negate this concern.

Pressure sensors used were of the type DST Centi TD (Star Oddi Ltd., Reykjavík, Iceland). These are also internally logging, and measure pressure with a resolution of 0.1 kPa (i.e., they can resolve approximately 1 cm changes of depth) and an accuracy of  $\pm 1$  kPa (i.e., approximately  $\pm 10$  cm water depth accuracy). The sensors were intercalibrated over a depth range of 0–8 m.

Atmospheric pressures were obtained from METAR (Meteorological Terminal Aviation Routine) reports generated hourly by the meteorological station at Lanvéoc-Poulmic Airbase (48° 16.93'N 4° 26.50'W). A time series with 2 min intervals was produced by interpolation. Atmospheric pressure was deducted from each measured pressure to isolate the component resulting from the overlying head of water alone. These values were converted to water depths by dividing by the product of water density and acceleration due to gravity. Water density was calculated according to the International Equation of State of Sea Water (IES-80) using measured pressures and temperatures (recorded by the DST Centi sensors as a secondary parameter), and an estimate of mean salinity at the site (34 psu is appropriate (Delmas 1981)). Acceleration due to gravity was calculated to be  $9.81 \text{ m s}^{-2}$  at the latitude of the Bay of Brest, using the International Gravity Formula (IGF).

### Numerical model

Numerical model input values (Table 1) were selected to represent the Bay of Brest, and an individual thallus of *Saccharina latissima* or an established macroalgal community growing there. A 1 h time step was used.

Sea surface irradiance,  $I_0(t)$ , was modeled over a year using the following equation (from Gates 1980):

$$I_0(N, t) = I_{\text{Atmos}}(N)\sin(\alpha(N, t))\exp[-k_{\text{Atmos}}m_{\text{Air}}(N, t)], \quad (9)$$

where  $I_{\text{Atmos}}$  is the solar irradiance incident upon a surface perpendicular to the Sun's rays just outside Earth's atmosphere (in this study we are interested only in the PAR component - see Table 1 footnote),  $\alpha$  is the solar altitude,  $k_{\text{Atmos}}$  is an atmospheric attenuation coefficient (which we have assumed to be a constant and have treated as a tunable parameter, and which represents a spectral average),  $m_{\text{Air}}$  is the air mass ratio,  $N$  is the day number ( $N = 0$  on January 1<sup>st</sup>), and  $t$  is time, measured in hours from the start of the day.

$I_{\text{Atmos}}$  varies over the year, as a result of the elliptical orbit of the Earth about the Sun, according to  $I_{\text{Atmos}}(N) = I_{\text{SC}}(1 + 0.0344\cos(360^\circ N/365))$  (Kreith and Kreider 1978; Duffie and

Beckman 2013), where  $I_{SC}$  is the solar constant - the irradiance (in this case, the PAR component only) received by a surface perpendicular to the Sun's rays just outside Earth's atmosphere at the mean Earth-Sun distance (see Table 1).

Solar altitude,  $\alpha$ , is the angular elevation of the Sun above the horizon, and was calculated using the equation first developed by Milankovitch (1930):  $\sin(\alpha(N, t)) = \sin(\gamma) \sin(\delta(N)) - \cos(\gamma) \cos(\delta(N)) \cos(360^\circ t/24)$ , where  $\gamma$  is the latitude (in degrees), and  $\delta$  is the solar declination (in degrees), the angle through which a given hemisphere is tilted toward (or away from) the Sun.  $\delta$  was, in turn, calculated using  $\delta(N) = 23.45 \sin(360^\circ(N+284)/365)$  (Cooper 1969; Brock 1981).

The air mass ratio,  $m_{Air}$ , is the ratio of the optical path length through the atmosphere in the direction of the Sun, at an angle of  $\alpha$ , to the path length in the vertical direction (i.e., with the Sun directly overhead at the zenith position) (Gates 1980). We employed the commonly used approximation (Gates 1980; Kumar et al. 1997) of  $m_{Air} = 1/\sin(\alpha)$ .

Equation 9 is essentially a restatement of the Lambert-Beer Law, with the irradiance arriving at the outer atmosphere being attenuated exponentially as it propagates toward the sea surface. The additional  $\sin(\alpha)$  factor, not found in the Lambert-Beer Law, represents an adjustment to  $I_{Atmos}$  (which is defined for a surface perpendicular to the Sun's rays) to account for the fact that extraterrestrial solar radiation may be obliquely incident upon the local zenith (see Gates (1980) for diagrams illustrating geometric considerations). The form of Eq. 9 results in a continuous sine wave output, from which only the non-negative values are of relevance to our northern hemisphere site. Negative values were set to zero by the model script to represent night-time irradiances, which may be considered negligible for our purposes.

Seabed irradiance time series (i.e.,  $I_{BT}(t)$  and  $I_{BNT}(t)$ ) were computed as  $I_0(t)$  attenuated exponentially by the product of water depth,  $z(t)$ , and diffuse attenuation coefficient of PAR,  $k_{PAR}(t)$ , again in accordance with the Lambert-Beer Law (Eq. 1).

To obtain "tidal" seabed irradiance,  $I_{BT}(t)$ , a tidally varying water depth was used. This was modeled as the sum of a lunar and a solar semi-diurnal tide (i.e., the  $M_2$  and  $S_2$  tidal constituents respectively), to produce a semi-diurnal and a springs-neaps cycle. The phase of the  $S_2$  constituent was set to  $180^\circ$  to ensure the low waters of spring tides always occurred at midday and midnight, as is approximately the case at the Bay of Brest.  $k_{PAR}(t)$  was modeled as daily mean values (i.e.,  $\bar{k}_{PAR}$ ) varying from day to day with daily mean tidal range,  $\bar{R}$ , as follows

$$\bar{k}_{PAR}(N) = \left( \frac{1}{2} + \frac{1}{2} \cos \frac{2\pi N}{365} \right) m\bar{R}(N) + c \quad (10)$$

where  $N$  is again day of the year, and  $m$  and  $c$  are constants. We return to the form of this equation below.  $\bar{R}(N)$  was modeled as a cosine function with a springs-neaps periodicity; the mean, amplitude, period and phase was set precisely by the  $M_2$  and  $S_2$

parameters in Table 1.  $k_{PAR}$  was not varied on shorter timescales (e.g., during the day with the semi-diurnal tide).

Irradiance and depth observations (see "Observational campaigns" section) together permitted the calculation of  $\bar{k}_{PAR}$  values for each day of the two campaigns (not shown). In winter, a scattered but statistically significant (at the 95% confidence level) positive linear relationship between  $\bar{k}_{PAR}$  and  $\bar{R}$  was observed. In summer, however, the relationship was not statistically significant (at the 95% confidence level). Hence, we modeled the variation of  $\bar{k}_{PAR}$  with  $\bar{R}$  over a year using Eq. 10, which is that of a straight line with an intercept,  $c$ , representing a base-line value of  $\bar{k}_{PAR}$ , and a gradient that varies incrementally throughout the year, from  $m$  in mid-winter (i.e.,  $\bar{k}_{PAR} = m\bar{R} + c$ ) to 0 in mid-summer (i.e.,  $\bar{k}_{PAR} = c$  for all  $\bar{R}$ ). The gradient variation between  $m$  and 0 is achieved by means of the bracketed "gradient modifier," a cosinusoidal function of annual periodicity, varying between 1 in mid-winter and 0 in mid-summer.  $m$  and  $c$  values used in the model are based on the winter observations, and are given in Table 1.

To obtain "non-tidal" seabed irradiance,  $I_{BNT}(t)$ , the mean water depth was applied at all times,  $t$ . The choice of  $k_{PAR}(t)$  parameterization was determined by the desired output. For daily amplification factors, daily mean values of  $k_{PAR}$  ( $\bar{k}_{PAR}$ ) were used here also (i.e.,  $k_{PAR}(t)$  was modeled, as for the "tidal" case, using Eq. 10). This is because the Bowers and Brubaker (2010) definition of daily tidal irradiance amplification requires that  $\bar{k}_{PAR}$  values used in both "tidal" and "non-tidal" cases be equal on any given day. For the output of springs-neaps amplification factors and for annual calculations, the "non-tidal"  $k_{PAR}$  was held constant (i.e., set to the mean of the  $\bar{k}_{PAR}$  values generated by Eq. 10) over each springs-neaps cycle or over the year, respectively.

Modeled  $I_{BT}(t)$  and  $I_{BNT}(t)$  were initially input into the Peeters and Eilers (1978)  $P-I$  Equation (Eq. 7) to provide  $P_{BT}(t)$  and  $P_{BNT}(t)$  appropriate at the thallus scale. Similarly, modeled  $I_{BT}(t)$  and  $I_{BNT}(t)$  were input into the Lederman and Tett (1981)  $P-I$  Equation (Eq. 8) to provide  $P_{BT}(t)$  and  $P_{BNT}(t)$  appropriate at the community scale. Daily, springs-neaps, and annual totals of these outputs, for use in calculating amplification factors, were determined by numerical integration (i.e., trapezium rule) with respect to time. Daily tidal amplification factors for irradiance,  $F$ , and photosynthesis,  $\Psi$ , were calculated according to Eqs. 2 and 5, respectively. Springs-neaps and annual irradiance and photosynthesis amplification factors (i.e.,  $F_{SN}$ ,  $\Psi_{SN}$ ,  $F_{ANN}$ , and  $\Psi_{ANN}$ ) were determined similarly:

$$F_{SN} = \frac{\langle I_{BT} \rangle_{SN}}{\langle I_{BNT} \rangle_{SN}}, \quad (11)$$

$$\Psi_{SN} = \frac{\langle P_{BT} \rangle_{SN}}{\langle P_{BNT} \rangle_{SN}}, \quad (12)$$

$$F_{ANN} = \frac{\langle I_{BT} \rangle_{ANN}}{\langle I_{BNT} \rangle_{ANN}}, \quad (13)$$

and

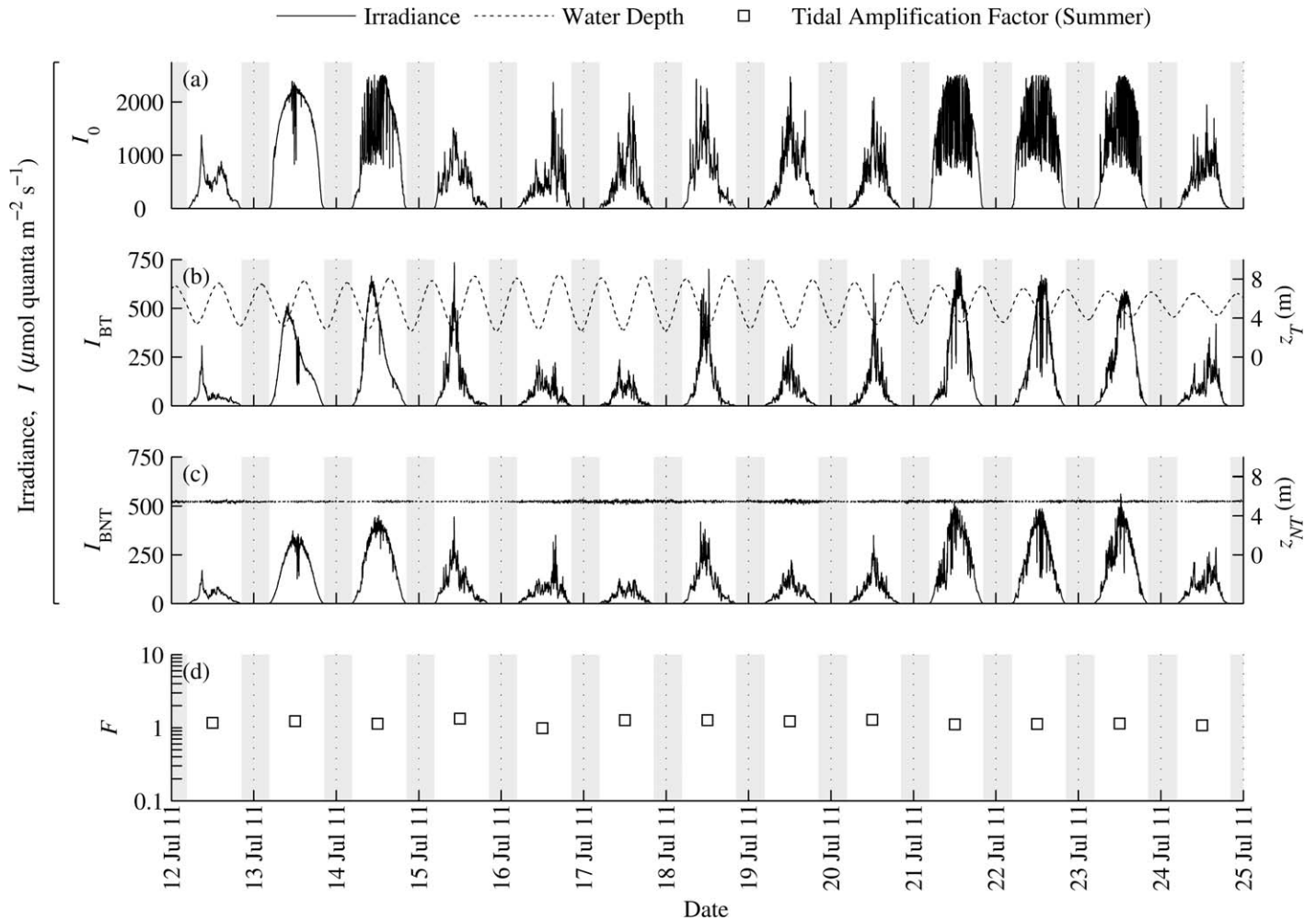


**Fig. 5.** Summer campaign time series data. Panel (a) shows sea surface irradiance,  $I_0$ ; (b) shows tidally modulated seabed irradiance,  $I_{BT}$ , and water depth,  $z_T$ , from the bed frame; and (c) shows “non-tidal” sub-surface irradiance,  $I_{BNT}$ , and water depth,  $z_{NT}$ , from the surface-moored frame. Panel (d) displays daily tidal irradiance amplification factors,  $F$ , determined in accordance with Eq. 2 (daily irradiance totals estimated by numerical integration using the trapezium rule). Note the  $\log_{10}$  scale used on the vertical axis. Gray-shaded areas represent night-time.

$$\Psi_{ANN} = \frac{\langle P_{BT} \rangle_{ANN}}{\langle P_{BNT} \rangle_{ANN}}, \quad (14)$$

where angular brackets with the subscripts  $SN$  or  $ANN$  denote springs-neaps or annual totals of the enclosed parameters, respectively.

## Results

### Tidal irradiance amplification determined from observations

Time series observations (see “Data availability statement” for access) and daily tidal irradiance amplification factors,  $F$ , from the summer and winter campaigns are presented in Figs. 5, 6, respectively. Throughout the summer campaign, observed  $F$  values were close to unity (Fig. 5d), ranging from 1.0 to 1.3. No clear springs-neaps cycle in  $F$  was apparent. In

the winter dataset, however,  $F$  values exhibited a strong springs-neaps cycle (Fig. 6d), being much larger at spring tides (up to 31.5) than at neap tides (as low as 0.4).

Agreement between observed and theoretically predicted tidal irradiance amplification (using Eq. 4) is demonstrated graphically in Fig. 7. The analytical solution appears to perform well for the Bay of Brest. Model II regression (i.e., the major axis method (Ricker 1973)) performed on the combined summer and winter data gave a slope of  $1.311 \pm 0.050$  and an intercept of  $-0.63 \pm 0.15$ .  $t$ -tests (two-tailed) were conducted to compare these values with the slope and intercept that would be expected in the case of perfect agreement between observations and predictions (i.e., 1 and 0, respectively). There were statistically significant differences (at the 95% confidence level) between both the slopes ( $t = 6.25$ ,  $df = 32$ ,  $p < 0.001$ ) and the intercepts ( $t = -4.10$ ,  $df = 32$ ,  $p < 0.001$ ). This departure from “perfect agreement” reflects

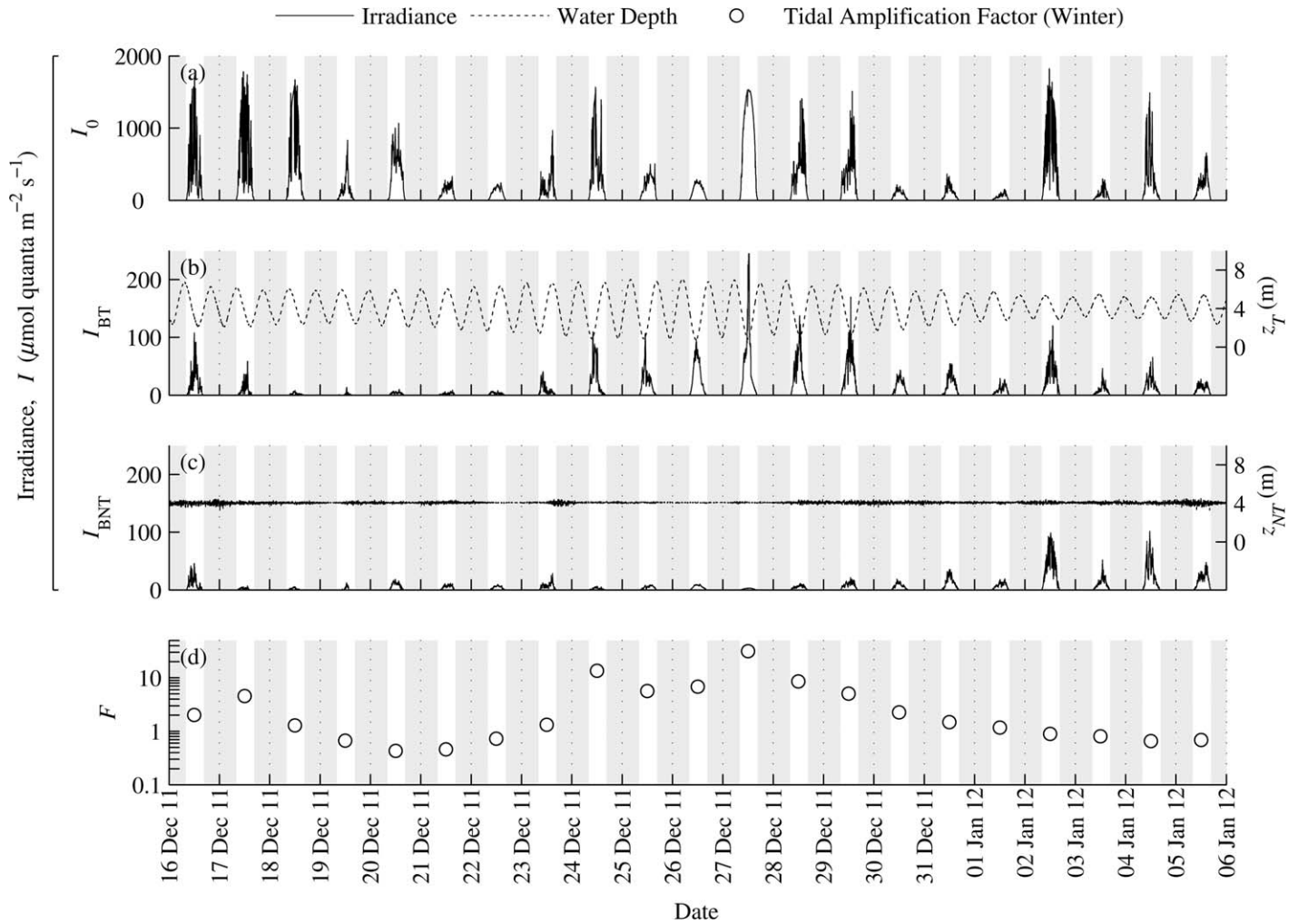


**Fig. 6.** Winter campaign time series data. Panel (a) shows sea surface irradiance,  $I_0$ ; (b) shows tidally modulated seabed irradiance,  $I_{BT}$ , and water depth,  $z_T$ , from the bed frame; and (c) shows “non-tidal” sub-surface irradiance,  $I_{BNT}$ , and water depth,  $z_{NT}$ , from the surface-moored frame. Panel (d) displays daily tidal irradiance amplification factors,  $F$ , determined in accordance with Eq. 2 (daily irradiance totals estimated by numerical integration using the trapezium rule). Note the  $\log_{10}$  scale used on the vertical axis. Gray-shaded areas represent night-time.

the relatively modest shortcomings of an analytical solution in which several assumptions were employed (*see* Bowers and Brubaker 2010). The solution shows a tendency to over-predict at larger amplifications.

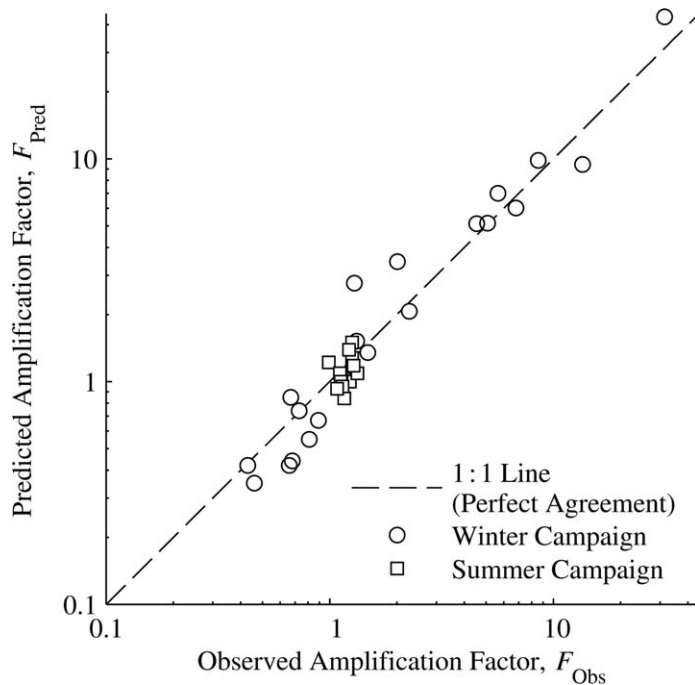
#### Tidal photosynthesis amplification determined from inferred photosynthesis

Figure 8 illustrates (using a subset of our irradiance time series observations, and rates of photosynthesis inferred from these observations), some conditions under which photosynthesis amplification factors,  $\Psi$ , and irradiance amplification factors,  $F$ , may converge or differ.

On 12<sup>th</sup> July (left hand panels, Fig. 8) overcast conditions ensure irradiances in both “tidal” and “non-tidal” scenarios remain below the saturation onset irradiance of an individual thallus for much of the day, and below that of an established community for the entire day. Consequently, photosynthesis

responds approximately linearly to irradiance throughout the day (in both “tidal” and “non-tidal” cases, and for both thallus and community). Computed thallus and community  $\Psi$  values are therefore both similar to the prevailing  $F$  value ( $F = 1.16$ , cf.  $\Psi(\text{thallus}) = 1.08$  and  $\Psi(\text{community}) = 1.11$ ).

On 13<sup>th</sup> July (right hand panels, Fig. 8) the sky was relatively cloud-free, and the day correspondingly brighter. Tidal irradiance amplification is clearly apparent by comparing the areas beneath the “tidal” and “non-tidal” irradiance curves. Thallus photosynthesis is light-saturated (and even photoinhibited) in both “tidal” and “non-tidal” scenarios for much of the day (note how  $P_B$  approximately flatlines in both scenarios between about 8 a.m. and 5 p.m.). There is no appreciable photosynthesis amplification at the thallus scale, and thus  $\Psi(\text{thallus})$  departs from  $F$  ( $F = 1.23$ , cf.  $\Psi(\text{thallus}) = 1.02$ ). In contrast, the  $P-I$  curve parameterization adopted here to describe community



**Fig. 7.** Predicted daily tidal irradiance amplification factors,  $F_{\text{Pred}}$ , generated using the Bowers and Brubaker (2010) analytical solution (Eq. 4), plotted against the observed values,  $F_{\text{Obs}}$ . Logarithmically scaled axes provide improved clarity at small  $F$  values, where all of the summer points and about half of the winter points are clustered. The dashed line represents the hypothetical case whereby theory and observation agree perfectly.

photosynthesis does not truly saturate, and inferred community photosynthesis continues to respond at these elevated irradiances. In the “tidal” community photosynthesis curve a local maximum can be seen at low water ( $\sim 9$  a.m.), and the curve is somewhat depressed around high water ( $\sim 3$  p.m.). Consequently, some tidal photosynthesis amplification occurs at the community scale, such that  $F$  and  $\Psi(\text{community})$  are closer in value ( $F = 1.23$ , cf.  $\Psi(\text{community}) = 1.11$ ).

#### Exploring the $F$ - $\Psi$ relationship with a numerical model

In Fig. 8, differences in sea surface irradiation from one day to the next, owing to differences in cloud cover, provided a convenient way to illustrate how  $F$  and  $\Psi$  may converge or differ. However, cloud cover is often ephemeral and changes with little temporal regularity. Here, we explore the more regular, predictable aspects of the  $F$ - $\Psi$  relationship using the simple numerical model described earlier (see “Materials and methods” section).

Output in which daily changes are resolved is shown in Fig. 9 for a mean water depth of 4.1 m (i.e., 1 m below the level of LWST) in the Bay of Brest. This corresponds approximately to the mean depth of our observations. Modeled  $F$  behavior (Fig. 9b) compares favorably with the winter and summer observations. A springs-neaps pattern in  $F$  is present

throughout the year; peaks are at spring tides (when low water is at midday) and troughs are at neaps (when high water is at midday). The amplitude of the cycle is large in winter (modeled  $F$  varies from 0.66 to 11.72), when short daylengths exaggerate the difference between springs and neaps. It is considerably reduced in summer (modeled  $F$  varies from 0.97 to 1.64), when the days are longer.

Modeled  $\Psi$  behavior at the thallus scale (Fig. 9c) corresponds with that of  $F$  in winter, but a “switch” in the sense of the springs-neaps pattern occurs near the equinoxes. Longer summer daylengths permit the morning and evening low waters of neap tides to occur within daylight hours. This boosts the tidally modulated photosynthesis (i.e.,  $P_{\text{BT}}$ ) at neaps. Consequently, they become more beneficial, in photosynthesis amplification terms, than spring tides, where a single, large pulse of seabed light around the midday low water saturates or inhibits  $P_{\text{BT}}$  (at this depth and time of year).

At the community scale, the springs-neaps cycle in  $\Psi$  does not “switch sense” to peak at neap tides during the summer months. Instead,  $\Psi$  “flatlines” at a value of approximately 1 throughout the summer (Fig. 9d). The mechanism responsible is the same as that invoked above to explain the “switch.” The effects are less dramatic for the case of macroalgal communities (i.e., a reduction, to nothing, of the amplitude of the springs-neaps cycle in  $\Psi$ , rather than a switch of sense) because communities do not become truly light-saturated or photoinhibited (Middelboe et al. 2006). Convergence of springs and neaps  $\Psi$  values upon a value of 1 during the summer months suggests that the tide has neither an amplifying or a reducing effect on community photosynthesis at these longer daylengths, and at this depth, in the Bay of Brest.

Figure 10 shows  $F_{\text{SN}}$ ,  $\Psi_{\text{SN}}$  (at the thallus scale), and  $\Psi_{\text{SN}}$  (at the community scale) modeled over a year at 1 m below the level of LWST in the Bay of Brest. At the thallus scale,  $F_{\text{SN}}$  and  $\Psi_{\text{SN}}$  do not correspond very closely; values of  $\Psi_{\text{SN}}$  (thallus) are suppressed by the increased prevalence of light-saturation and photoinhibition in this scenario. In the summer, tidal (i.e., springs-neaps) reduction of thallus photosynthesis occurs (i.e.,  $\Psi_{\text{SN}}(\text{thallus}) < 1$ ), despite tidal amplification of irradiance (i.e.,  $F_{\text{SN}} > 1$ ).

At the community scale, the magnitudes and temporal behavior of  $\Psi_{\text{SN}}$  more closely approach those of  $F_{\text{SN}}$ . No appreciable tidal reduction of photosynthesis is sustained through summer. This can again be explained by the absence of true light-saturation in the community-scale  $P$ - $I$  curve parameterization. Even the largest maxima in tidally modulated seabed irradiance, occurring at (the midday) LWST during summer, do not present a macroalgal community with such a “photosynthetic disadvantage” (i.e., prolonged saturation or photoinhibition) as they do an individual/isolated kelp thallus in shallow water.

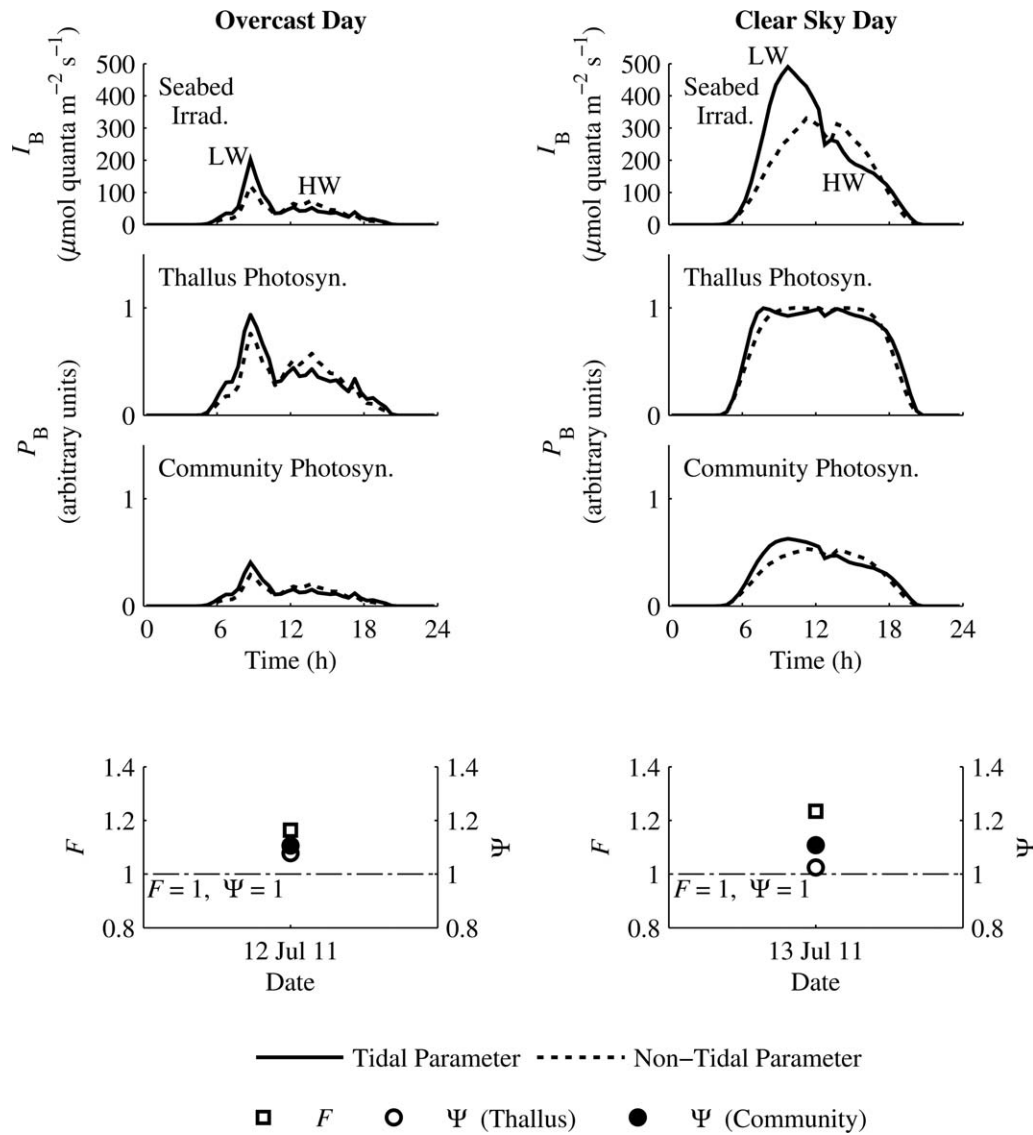


**Fig. 8.** Conditions under which photosynthesis amplification factors,  $\Psi$ , and irradiance amplification factors,  $F$ , may converge (left hand panels) or differ (right hand panels). See text for explanation. Irradiances are observed values (30 min averages). Rates of photosynthesis are inferred using the relevant  $P-I$  equations (see Theory). Times of low and high waters are denoted by LW and HW respectively in the uppermost panels.

The annual tidal irradiance amplification factor,  $F_{ANN}$ , output by the model for a depth of 1 m below the level of LWST in the Bay of Brest was 2.33. The annual photosynthesis amplification factors at the thallus and community scales,  $\Psi_{ANN}(\text{thallus})$  and  $\Psi_{ANN}(\text{community})$ , for the same depth were 1.06 and 1.42, respectively.

### Discussion

#### Observations in the Bay of Brest

The key physical parameters controlling the magnitude of the tidal irradiance amplification effect (on a given day) were identified by Bowers and Brubaker (2010) to be the

diffuse attenuation coefficient,  $k_{PAR}$ , the tidal range,  $R$  (or amplitude,  $b$ ), the times of low water relative to noon,  $t_{lw}$ , and the daylength,  $L$ . In a qualitative sense, our observations in the Bay of Brest support this. In winter, the amplification is large at springs when  $R$  is large,  $k_{PAR}$  is elevated generally, and low water occurs at midday. Reduction occurs at neaps when  $R$  and  $k_{PAR}$  are smaller, and high water occurs at midday. This springs-neaps pattern appears to be modulated also by the seasonal cycle in daylength: it is pronounced in winter, when short days exaggerate the consequences of having either low water or high water at midday (i.e., springs and neaps respectively); it is not present in summer, when longer days permit the irradiance “gains” of the midday LWST, or

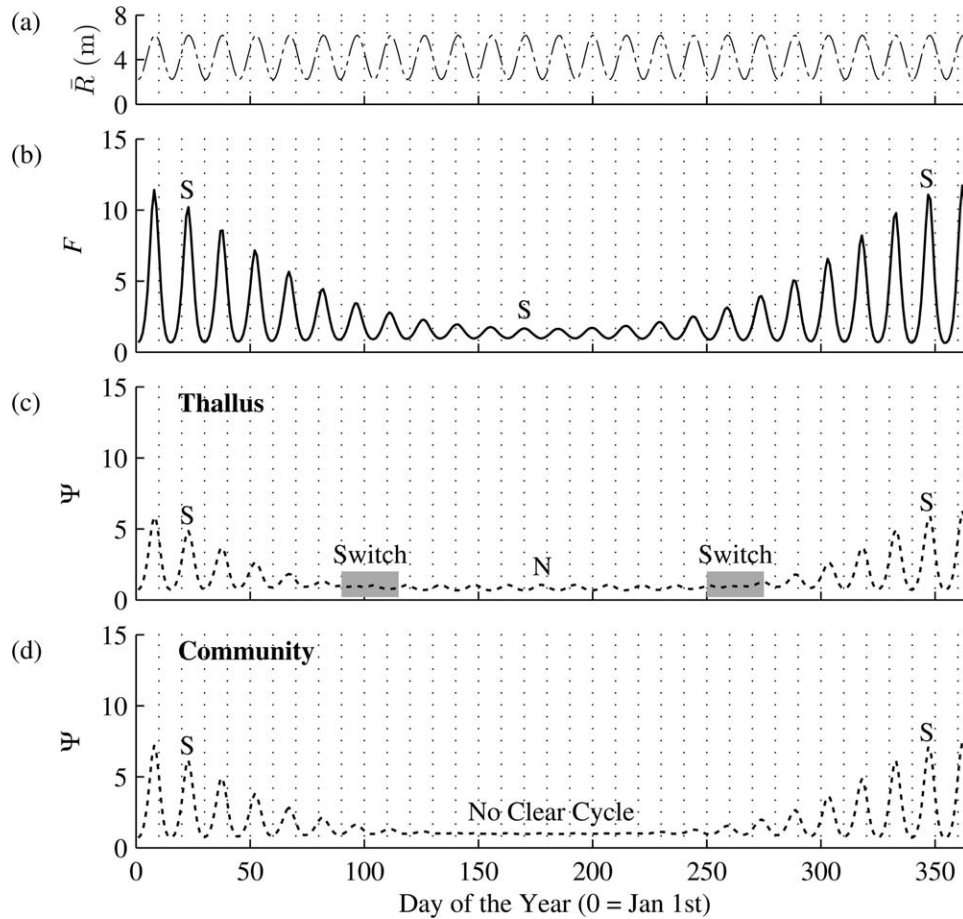


**Fig. 9.** Numerical model output over a year at 1 m below the level of LWST. Panel (a) shows daily mean tidal range,  $\bar{R}$ , and its springs-neaps variation, for reference, (b) shows the daily tidal irradiance amplification factor,  $F$ , (c, d) show the analogously defined daily tidal photosynthesis amplification factor,  $\Psi$ , determined at the thallus and community scales, respectively. Peaks in  $F$  and  $\Psi$  are labeled S (springs) or N (neaps) to denote the sense of cycles at various times of year. The sense “switching” behavior of cycles in  $\Psi$  at the thallus scale, and the lack thereof at the community scale, is discussed in the text. Input values were representative of the Bay of Brest, and of a thallus of *Saccharina latissima* (in the case of (c)) or an established macroalgal community (in the case of (d)).

“losses” of the midday high water neap tide (HWNT), to be offset somewhat by the morning and evening high waters, or low waters, respectively.

Agreement between existing theory and observation has, in this paper, been demonstrated quantitatively also. Comparison of observed daily tidal irradiance amplification factors,  $F_{\text{Obs}}$ , with those predicted for the conditions on each day,  $F_{\text{Pred}}$ , using the analytical solution of Bowers and Brubaker (2010) (a function of the four key parameters outlined above) shows reasonable agreement. Much of the key physics underlying tidal amplification is included in the analytical solution and, based on the fact that it has performed well for two sites with contrasting tidal regimes (i.e., the Menai Strait in the earlier work (Bowers and Brubaker 2010) and the Bay of Brest in the current work), it can be expected to perform at least reasonably well for many more, perhaps most, coastal sites with a semi-diurnal tide.

As a caveat to the above, we note that a tidal cycle in  $k_{\text{PAR}}$  is present at the Bay of Brest (not shown in this paper). As for the Menai Strait (Roberts et al. 2014) and the Tamar Estuary (Pilgrim and Millward 1989, and references therein), the cycle is out of phase with the tidal curve, reaching a maximum at low water and a minimum at high water. The Bowers and Brubaker (2010) solution assumes constant  $k_{\text{PAR}}$  over the day, and employs the daily mean value in predicting  $F$ . This was necessary in order to make the analytical solution possible. The consequence is that the solution tends to overpredict  $F$  on days where the  $k_{\text{PAR}}$  tidal cycle is particularly distinct (e.g., on 27<sup>th</sup> December  $F_{\text{Obs}} = 31.5$ , whereas  $F_{\text{Pred}} = 43.4$  (see Figs. 6, 7)).

While we have insufficient data to say anything conclusive about the nature of the mechanism driving the tidal cycle in  $k_{\text{PAR}}$ , we speculate, as did Pilgrim and Millward (1989), that it involves the local resuspension of sediment

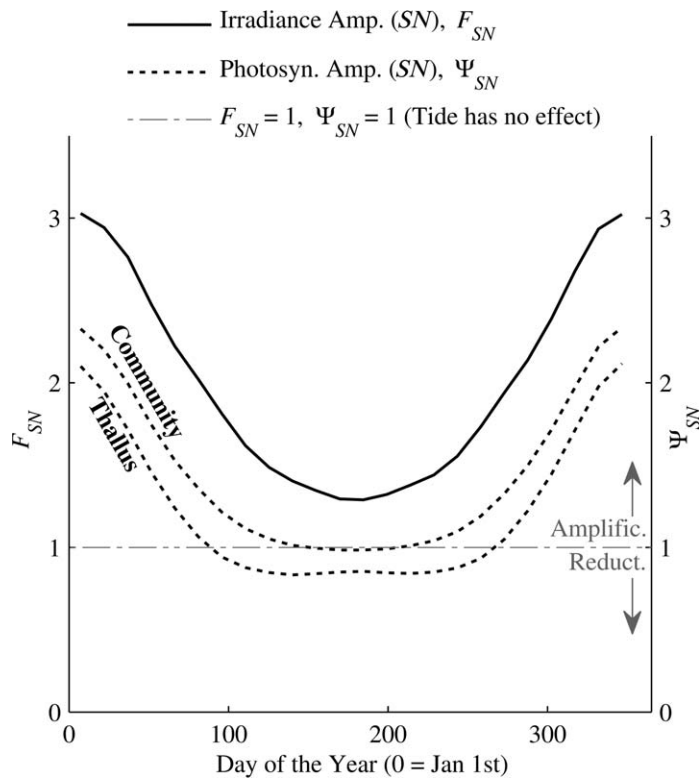


**Fig. 10.** Springs-neaps irradiance amplification factors,  $F_{SN}$ , and springs-neaps photosynthesis amplification factors,  $\Psi_{SN}$ , output by the numerical model for a depth of 1 m below LWST in the Bay of Brest. Two  $\Psi_{SN}$  curves are shown, representing model runs with  $P-I$  parameterizations appropriate at the thallus scale and at the community scale. The dash-dotted line indicates the threshold above which amplification is said to have occurred and below which reduction has occurred.

by increased turbulence at low water. It could, therefore, be common to many shallow, coastal sites. At other sites,  $k_{PAR}$  behavior may exhibit clear cycles with quarter-diurnal or semi-diurnal frequency, owing to tidal resuspension or tidal advection of suspended particulate matter (SPM) respectively (e.g., Weeks et al. 1993; Williams et al. 1998). In any case, an analytical solution of comparable simplicity to that of Bowers and Brubaker (2010), which incorporates such regular patterns in  $k_{PAR}$ , is difficult to achieve. Use of the Bowers and Brubaker (2010) solution to make predictions for sites with appreciable and inherent  $k_{PAR}$  cycles will incur some error, and the interested investigator is advised to model the tidal irradiance amplification effect (including the  $k_{PAR}$  variability) numerically in these cases.

An irradiance sensor in a simple bed frame provided the “tidal” irradiance data in the present work, whereas a novel mooring was designed and employed to allow irradiance in the hypothetically equivalent “non-tidal” condition to be measured directly, rather than inferred from surface irradiance records. This new mooring performed encouragingly well: it provided high quality, continuous time series data

for each campaign; it did not become entangled, despite tidal currents and, occasionally, strong wind forcing; and, most importantly, it successfully held the irradiance sensor at a relatively constant water depth over time.

Two limitations are associated with the use of this mooring. First, while the irradiance data is rendered independent of tidal variations in water depth by the mooring, it is not independent of the tidal variations in  $k_{PAR}$  discussed above. Thus, it is not comprehensively “non-tidal” data but, given that the tidal range in the Bay of Brest is typically much greater than the range in  $k_{PAR}$ , it is sufficiently so for our purposes. Second, the “non-tidal” mooring was deployed further offshore than the “tidal” bed frame. This allowed the requirement of equal mean depths to be satisfied, while preventing the “non-tidal” sensor from becoming grounded at low water. As a consequence, the daily mean  $k_{PAR}$  (i.e.,  $\bar{k}_{PAR}$ ), as experienced by the “non-tidal” sensor, was consistently lower than at the shallower “tidal” bed frame site. This is not desirable ( $\bar{k}_{PAR}$  should be approximately equal in both conditions) and necessitated the application of a Lambert-Beer-based correction (see “Materials and methods” section) to the “non-tidal” data.

A workaround exists for the second limitation: deploy the bed frame further offshore also, elevating its sensor considerably to maintain the same mean depth. This is logistically much less practical, however, both in terms of the deployability of the adapted (larger) frame and of the increased danger to shipping in these relatively busy, shallow waters.

### Numerical modeling predictions

The following key predictions emerged out of the modeling study, and apply to the shallow sub-tidal (i.e., 1 m below the level of LWST) in the Bay of Brest:

- Annual total seabed irradiance is amplified by the tide (by a factor of 2.33 relative to a “non-tidal” but otherwise equivalent scenario). Annual total photosynthesis at the seabed is hardly amplified at all by the tidal irradiance amplification (i.e., by a factor of just 1.06) at the isolated, individual thallus scale, but it is more substantially amplified at the established macroalgal community scale (i.e., by a factor of 1.42).
- When considered at springs-neaps resolution, tidal modulation of seabed irradiance is of greatest significance, in terms of its influence on the photosynthesis of benthic algae, during winter (when it results in amplification of photosynthesis at both community and thallus scales). It is of less significance during summer, when it has a negligible effect at the community scale and results in a modest, sustained reduction in photosynthesis at the thallus scale.
- At finer temporal resolution, a springs-neaps cycle is present in the daily tidal irradiance amplification factor. Peaks are at spring tides, troughs are at neap tides, and the amplitude of the cycle is large in winter and considerably

smaller in summer (in agreement with our observations). The daily tidal photosynthesis amplification factor exhibits a similar pattern during winter at both the thallus and community scales. During summer, however, this pattern “switches sense” (such that the peaks are at neap tides) at the thallus scale, and “flatlines” (at a value of approximately 1) at the community scale.

As noted previously, the springs-neaps cycle in daily tidal irradiance amplification factor peaks at spring tides because a low water occurs at about midday during springs at the Bay of Brest. Conversely, troughs are at neap tides because a high water occurs at midday at these times. The amplitude of the cycle is larger in winter because shorter daylengths exaggerate the difference between these two situations. The irradiance-amplifying potential of spring tides in winter also accounts for amplification predicted over longer timescales (i.e., the amplification occurring during winter at the springs-neaps timescale, and the overall annual amplification).

Whether tidal amplification of seabed light produces a similar amplification of seabed photosynthesis depends on how light levels compare with the saturation onset irradiance of a given species or community. Below this threshold, rates of photosynthesis respond approximately linearly to the time course of instantaneous irradiance, and photosynthesis amplification corresponds with the prevailing irradiance amplification. Should irradiances exceed this threshold (as occurs more frequently in summer), the relationship between irradiance amplification and photosynthesis amplification becomes more complex, and (as we have shown) their respective factors may differ. The response of the isolated, individual thallus and that of the established macroalgal community will differ in this respect because their photosynthesis-irradiance characteristics are different (Gévaert et al. 2003; Middelboe et al. 2006): a kelp thallus may become light-saturated and even photoinhibited, but an established macroalgal community is unlikely to become truly light-saturated. Generally, the consequence is that, at the thallus scale, photosynthesis amplification factors readily depart from their corresponding irradiance amplification factors (including the case whereby photosynthesis is reduced despite irradiance being amplified by the tide), while at the community scale, there is likely to be a more consistently positive correlation between tidal irradiance amplification and photosynthesis amplification.

The numerical model was constructed using widely accepted parameterizations of key physical and biological processes. For example, surface irradiance was modeled using well-known equations found in Gates (1980), Kirk (1994), and others, the attenuation of irradiance with water depth was modeled using the Lambert-Beer Law, tidally varying water depth was modeled as the sum of two sinusoidal tidal constituents ( $M_2$  and  $S_2$ ), and  $P-I$  curves were modeled with the Peeters and Eilers (1978) Equation (appropriate at the thallus scale) and the Lederman and Tett (1981) Equation

(appropriate at the community scale). The main limitations of the work are associated with the use of photosynthesis parameters, controlling the precise shape of the  $P-I$  curves, that are unchanging over time.

In fact, the shape of a  $P-I$  curve exhibits a dependence on water temperature and substrate (i.e.,  $\text{CO}_2$ ) availability, both of which are liable to change, to varying degrees, over the timescales considered here (Dring 1992; Hurd et al. 2014). Furthermore, a  $P-I$  curve can be temporally dynamic owing to mechanisms endogenous to the alga, particularly those which permit it to maximize its performance in any situation (Delebecq et al. 2013). Notably, algae are known to acclimate to changes in the intensity and spectral quality of the ambient light, on timescales ranging from minutes to months, by adjustments to their photosynthetic apparatus (Dring 1992; Kirk 1994; Falkowski and Raven 1997; Hurd et al. 2014). Short-term adjustments (e.g., minutes to days) include changes to the Photosystem II absorption cross-section, changes to the position and orientation of chromatophores, and photoprotective mechanisms, such as non-photochemical quenching (i.e., the harmless dissipation of excess light energy as heat) (Nultsch and Pfau 1979; Müller et al. 2001; Duarte et al. 2013). Longer-term adjustments (e.g., days to months) include changes to pigment content and composition (Kirk 1994).

Duarte et al. (2013) noted that  $P-I$  curve parameters should be considered as variables rather than constants. As discussed, these variables are functions of many environmental parameters (e.g., temperature,  $\text{CO}_2$  concentration, ambient light intensity, and quality) and have, as yet, not been parameterized satisfactorily. We chose to employ “static,” or fixed,  $P-I$  curves taken from the literature when modeling photosynthesis over time from modeled irradiance (as did Zimmerman et al. 1994). While this is likely to be a reasonable first order approximation (see Middelboe et al. 2006), the accuracy of model estimates/predictions will undoubtedly be improved if studies like those of Gévaert et al. (2003) and Duarte et al. (2013) can be built upon to provide generalizable parameterizations of a  $P-I$  curve’s “dynamic” nature.

There are a number of broad implications of the modeling study that can be extended to sites other than the Bay of Brest. Demonstrated for the first time in this work, the effect of the tide in amplifying or reducing time-integrated seabed light is likely to induce a similar effect on time-integrated benthic photosynthesis. These effects are likely to be more strongly coupled at the macroalgal community scale (which is arguably more ecologically relevant than that of the isolated thallus). To extend comments made by Bowers and Brubaker (2010), just as error will be introduced to modeled estimates of seabed light if tidal effects are neglected, for example by employing a mean water depth and clarity over time, the same is likely to be true of modeled estimates of seabed photosynthesis. At many sites, neglecting the tidal effects will lead to underestimates of time-integrated irradiance and photosynthesis in the subtidal zone.

We have shown that the time course of benthic photosynthesis and time-integrated benthic photosynthesis in the shallow subtidal appear to be controlled, at least in part, by the tidal characteristics of the site in question, through their modulation of seabed irradiance (i.e., the times of low water,  $t_{lw}$ , and their advance through the springs-neaps cycle, and the tidal range,  $R$ , and its variability). Observed differences in these aspects of benthic photosynthesis from site to site may be attributable to differences in  $t_{lw}$ ,  $R$ ,  $k_{PAR}$  and  $L$  behavior between the sites, rather than (or in addition to) abiotic and biotic factors identified in the literature to date.

We speculate that there may be a second important spatial (i.e., depth) component to the effect of tidal modulation of seabed light on benthic photosynthesis and ecology. Since subtidal benthic algae are readily light-limited, and different species possess different light requirements/tolerances, it is natural to hypothesize that such an effect might influence the depth distribution of these species differentially, in turn influencing characteristics of the prevailing benthic community such as depth gradients in species composition, vertical zonation patterns, and overall areal extent and algal cover. A modeling approach such as the one adopted here cannot be employed to investigate this until the effects of photoacclimation on photosynthesis parameters (in the depth dimension) have been adequately quantified and parameterized for key species. This is a problem of considerable importance to the field of modeling shallow-water benthic productivity, and is our primary recommendation as a direction for future research.

In terms of the practical relevance of this work, habitat managers and policy makers should be aware that projects which alter the tidal characteristics of a particular coastline, such as the construction of barrages or lagoons for tidal energy extraction, and the changes to tides that are predicted to occur with sea-level variability (e.g., Neill et al. 2010) are likely to affect the time course of photosynthesis in, and the overall productivity of, benthic plants and algae, through the tide's influence on the available seabed light.

### Data availability statement

Seabed and sea surface light time series records (and associated water depth and temperature records) are available at [https://www.bodc.ac.uk/data/published\\_data\\_library/catalogue/10.5285/4fc90854-3754-29a2-e053-6c86abc0af53/](https://www.bodc.ac.uk/data/published_data_library/catalogue/10.5285/4fc90854-3754-29a2-e053-6c86abc0af53/)

### References

- Ackleson, S. G. 2003. Light in shallow waters: A brief research review. *Limnol. Oceanogr.* **48**: 323–328. doi:10.4319/lo.2003.48.1\_part\_2.0323
- Bowers, D. G., P. Tett, and A. W. Walne. 1997. A note on seabed irradiance in shallow tidal seas. *J. Mar. Biol. Assoc. U.K.* **77**: 921–928. doi:10.1017/S0025315400038534
- Bowers, D. G., and J. M. Brubaker. 2004. Underwater sunlight maxima in the Menai Strait. *J. Opt. A* **6**: 684–689. doi:10.1088/1464-4258/6/7/005
- Bowers, D. G., and J. M. Brubaker. 2010. Tidal amplification of seabed light. *J. Geophys. Res.* **115**: C09008. doi:10.1029/2009JC005785
- Brock, T. D. 1981. Calculating solar radiation for ecological studies. *Ecol. Modell.* **14**: 1–19. doi:10.1016/0304-3800(81)90011-9
- Cooper, P. I. 1969. The absorption of solar radiation in solar stills. *Solar Energy* **12**: 333–346. doi:10.1016/0038-092X(69)90047-4
- Delebecq, G., D. Davoult, D. Menu, M. A. Janquin, J. C. Dauvin, and F. Gévaert. 2013. Influence of local environmental conditions on the seasonal acclimation process and the daily integrated production rates of *Laminaria digitata* (Phaeophyta) in the English Channel. *Mar. Biol.* **160**: 503–517. doi:10.1007/s00227-012-2106-3
- Delmas, R. 1981. Étude de l'évolution saisonnière des sels nutritifs dans la rade de Brest en fonction des apports fluviaux et des échanges avec l'Iroise. Ph.D. thesis. Université de Bretagne Occidentale.
- Delmas, R., and P. Tréguer. 1983. Évolution saisonnière des nutriments dans un écosystème eutrophe d'Europe Occidentale (la rade de Brest). *Interactions marines et terrestres. Oceanol. Acta* **6**: 345–355.
- Dring, M. J. 1992. *The biology of marine plants*. Cambridge Univ. Press.
- Duarte, P., M. Ramos, G. Calado, and B. Jesus. 2013. *Laminaria hyperborea* photosynthesis-irradiance relationship measured by oxygen production and pulse-amplitude-modulated chlorophyll fluorometry. *Aquat. Biol.* **19**: 29–44. doi:10.3354/ab00515
- Duffie, J. A., and W. A. Beckman. 2013. *Solar engineering of thermal processes*, 4th ed. John Wiley and Sons.
- Falkowski, P. G., and J. A. Raven. 1997. *Aquatic photosynthesis*. Blackwell.
- Gates, D. M. 1980. *Biophysical ecology*. Springer-Verlag New York.
- Gévaert, F., A. Créach, D. Davoult, A. C. Holl, L. Seuront, and Y. Lemoine. 2002. Photo-inhibition and seasonal photosynthetic performance of the seaweed *Laminaria saccharina* during a simulated tidal cycle: Chlorophyll fluorescence measurements and pigment analysis. *Plant Cell Environ.* **25**: 859–872. doi:10.1046/j.1365-3040.2002.00869.x
- Gévaert, F., A. Créach, D. Davoult, A. Migné, G. Levavasseur, P. Arzel, A. C. Holl, and Y. Lemoine. 2003. *Laminaria saccharina* photosynthesis measured in situ: Photoinhibition and xanthophyll cycle during a tidal cycle. *Mar. Ecol. Prog. Ser.* **247**: 43–50. doi:10.3354/meps247043
- Heck, K. L., G. Hays, and R. J. Orth. 2003. Critical evaluation of the nursery role hypothesis for seagrass meadows. *Mar. Ecol. Prog. Ser.* **253**: 123–136. doi:10.3354/meps253123
- Hily, C., P. Potin, and J. Y. Floc'h. 1992. Structure of subtidal algal assemblages on soft-bottom sediments: Fauna/flora interactions and role of disturbances in the Bay of Brest, France. *Mar. Ecol. Prog. Ser.* **85**: 115–130. doi:10.3354/meps085115
- Hurd, C. L., P. J. Harrison, K. Bischof, and C. S. Lobban. 2014. *Seaweed ecology and physiology*. Cambridge Univ. Press.

- Kirk, J. T. O. 1994. Light and photosynthesis in aquatic ecosystems, 2nd ed. Cambridge Univ. Press.
- Kreith, F., and J. F. Kreider. 1978. Principles of solar engineering. McGraw-Hill.
- Kumar, L., A. K. Skidmore, and E. Knowles. 1997. Modelling topographic variation in solar radiation in a GIS environment. *Int. J. Geogr. Inf. Sci.* **11**: 475–497. doi:10.1080/136588197242266
- Lederman, T. C., and P. Tett. 1981. Problems in modelling the photosynthesis-light relationship for phytoplankton. *Bot. Mar.* **24**: 125–134. doi:10.1515/botm.1981.24.3.125
- Mann, K. H. 1972. Ecological energetics of the sea-weed zone in a marine bay on the Atlantic coast of Canada. II. Productivity of the seaweeds. *Mar. Biol.* **14**: 199–209. doi:10.1007/BF00348280
- Middelboe, A. L., K. Sand-Jensen, and T. Binzer. 2006. Highly predictable photosynthetic production in natural macroalgal communities from incoming and absorbed light. *Oecologia* **150**: 464–476. doi:10.1007/s00442-006-0526-9
- Milankovitch, M. 1930. Mathematische klimalehre und astronomische theorie der klimaschwankungen. In W. Köppen and R. Geiger (Eds.), *Handbuch der Klimatologie*, Band I, Teil A. Gebrüder Borntraeger.
- Monbet, Y., and P. Bassoullet. 1989. Bilan des connaissances océanographiques en rade de Brest. Rapport CEA/IPSN, code DERO/EL 89-23, IFREMER-DEL-BP 70-29280. Technical Report. IFREMER. Plouzané.
- Müller, P., X. P. Li, and K. K. Niyogi. 2001. Non-photochemical quenching. A response to excess light energy. *Plant Physiol.* **125**: 1558–1566. doi:10.1104/pp.125.4.1558
- Naylor, E. 2010. Chronobiology of marine organisms. Cambridge Univ. Press.
- Neill, S. P., J. D. Scourse, and K. Uehara. 2010. Evolution of bed shear stress distribution over the northwest European shelf seas during the last 12,000 years. *Ocean Dyn.* **60**: 1139–1156. doi:10.1007/s10236-010-0313-3
- Nultsch, W., and J. Pfau. 1979. Occurrence and biological role of light-induced chromatophore displacements in seaweeds. *Mar. Biol.* **51**: 77–82. doi:10.1007/BF00389033
- Peeters, J. C. H., and P. Eilers. 1978. The relationship between light intensity and photosynthesis - a simple mathematical model. *Hydrobiol. Bull.* **12**: 134–136. doi:10.1007/BF02260714
- Pilgrim, D. A., and G. E. Millward. 1989. Variation in the diffuse optical depth of the bed of a tidal estuary, p. 101–107. In J. McManus and M. Elliott [eds.], *Developments in estuarine and coastal study techniques*. Olsen and Olsen.
- Pingree, R. D., and D. K. Griffiths. 1981. S2 tidal simulations on the north-west European shelf. *J. Mar. Biol. Assoc. U.K.* **61**: 609–616. doi:10.1017/S0025315400048074
- Ricker, W. E. 1973. Linear regressions in fishery research. *J. Fish. Res. Board Canada* **30**: 409–434. doi:10.1139/f73-072
- Roberts, E. M. 2015. Tidal modulation of seabed light and its implications for benthic algae. Ph.D. thesis. Bangor Univ.
- Roberts, E. M., D. G. Bowers, and A. J. Davies. 2014. Springs-neaps cycles in daily total seabed light: Daylength-induced changes. *J. Mar. Syst.* **132**: 116–129. doi:10.1016/j.jmarsys.2014.01.009
- Salomon, J. C., and M. Breton. 1991. Numerical study of the dispersive capacity of the Bay of Brest, France, towards dissolved substances, p. 459–464. In J. H. W. Lee and Y. K. Cheung [eds.], *Environmental hydraulics*. Balkema.
- Steneck, R. S., M. H. Graham, B. J. Bourque, D. Corbett, J. M. Erlandson, J. A. Estes, and M. J. Tegner. 2002. Kelp forest ecosystems: Biodiversity, stability, resilience and future. *Environ. Conserv.* **29**: 436–459. doi:10.1017/S0376892902000322
- Thouzeau, G., L. Chauvaud, J. Grall, and L. Guérin. 2000. Rôle des interactions biotiques sur le devenir du pré-recrutement et la croissance de *Pecten maximus* (L.) en rade de Brest. *C. R. Acad. Sci. III* **323**: 815–825. doi:10.1016/S0764-4469(00)01232-4
- Topliss, B. J., J. R. Hunter, and J. H. Simpson. 1980. Simultaneous measurements of transparency and irradiance in the coastal waters of North Wales. *Mar. Environ. Res.* **4**: 65–79. doi:10.1016/0141-1136(80)90060-4
- Weeks, A. R., J. H. Simpson, and D. G. Bowers. 1993. The relationship between concentrations of suspended particulate material and tidal processes in the Irish Sea. *Cont. Shelf Res.* **13**: 1325–1334. doi:10.1016/0278-4343(93)90086-D
- Williams, J. J., J. D. Humphery, P. J. Hardcastle, and D. J. Wilson. 1998. Field observations of hydrodynamic conditions and suspended particulate matter in the southern North Sea. *Cont. Shelf Res.* **18**: 1215–1233. doi:10.1016/S0278-4343(98)00041-7
- Zimmerman, R. C., A. Cabello-Pasini, and R. S. Alberte. 1994. Modeling daily production of aquatic macrophytes from irradiance measurements: A comparative analysis. *Mar. Ecol. Prog. Ser.* **114**: 185–196. doi:10.3354/meps114185

#### Acknowledgments

Fieldwork in Brest was made possible thanks to the following people: Georges Chapalain, Alexis Beudin, and Antoine Douchin, of CETMEF (now Cerema); IUEM (Institut Universitaire Européen de la Mer) scientists and technicians working on the CHIVAS (Chimie des Valves de la Coquille Saint-Jacques Européennes) project; and the captain and crew of RV *Albert Lucas*. Mervyn and Susan Roberts, and Yvon and Christiane Lainé kindly provided logistical support and accommodation. Malen Jukes and Geraint Roberts are thanked for commenting on the manuscript. Two anonymous reviewers are thanked for their suggestions, which led to considerable improvements to this work. This work was supported by the Natural Environment Research Council [Grant Number NE/1527853/1].

#### Conflict of Interest

None declared.

Submitted 08 June 2016

Revised 21 November 2016; 06 March 2017

Accepted 04 May 2017

Associate editor: Núria Marbà